$\label{eq:continuous_problem} \textbf{Detailed Kinetic Modeling of NO}_{X} \!\!-\!\! \textbf{Mediated Oxidative Dehydrogenation of Propane}$

Peng Yu^a, Yilang Liu^b, Prashant Deshlahra^b, and Hsi-Wu Wong^{a*}

^aDepartment of Chemical Engineering, University of Massachusetts Lowell

One University Avenue, Lowell, MA, 01854, USA

^bDepartment of Chemical and Biological Engineering, Tufts University

4 Colby Street, Medford, MA, 02155, USA

ABSTRACT: Shale gas is revitalizing America's chemical industry and shifting ethylene

production from oil-based naphtha to shale-derived ethane, causing a short supply of propylene.

Oxidative dehydrogenation of propane mediated by NO_X (NO and NO₂) provides a potential route

to convert propane into propylene without solid catalysts. In this work, detailed kinetic modeling

was performed to simulate gas-phase homogeneous NO_X-mediated oxidative dehydrogenation of

propane. Consistent with the experimental findings, our model suggests that propane conversion

increases with the amount of NO in the feed, with the selectivity to propylene and ethylene

decreased with increasing propane conversion. Our modeling results also revealed that OH radicals

are the major species to consume propane. The addition of NO_X in the system increases the

production of OH radicals due to additional pathways in the NO-NO2 cycle, including (1)

oxidation of NO by HO₂ radicals, (2) reduction of NO₂ by H radicals, and (3) formation and

dissociation of HONO and its isomers, facilitating propylene formation. The addition of H₂O

further accelerates propane conversion by shifting the equilibrium of OH quenching reactions. A

reaction network consisting of propane pyrolysis, propane oxidative dehydrogenation, and NO_X

mediation was sketched to explain the important trends observed in the experiments.

*Corresponding author: Hsi-Wu Wong, +1 (978) 954-5290, Email: hsiwu wong@uml.edu

Introduction

Shale gas is revitalizing America's chemical industry and now the United States enjoys a decisive competitive edge in petrochemical production. Access to vastly new supply of natural gas and natural gas liquids (i.e., ethane, propane, and butane) from shale is one of the most exciting developments in the United States during the past ten years. For example, the production of shale gas in the Appalachian region, including Ohio, Pennsylvania, West Virginia, and Kentucky, is so abundant that, if it were an independent country, the region would be the world's third largest producer of natural gas. Newly discovered shale resources also allow ethane-based steam cracking to become a more inexpensive route for producing high value chemicals (HVCs) than conventional naphtha steam cracking; for instance, the cost of ethane is one third lower than that of naphtha in the U.S. in 2017. For these reasons, increasingly more chemical companies are moving away from using naphtha as a feedstock to produce HVCs. This shift, however, is leading to a short supply of propylene due to lack of technologies to directly convert shale-derived propane into propylene.

To resolve this challenge, several on–purpose propylene (OPP) production technologies⁶ have been proposed. Catalytic propane dehydrogenation is the most common OPP approach, where extensive research has been focusing on the optimization of catalyst performance.⁷⁻¹² Another approach is catalytic oxidative dehydrogenation of propane, where higher propane conversion could be achieved in the presence of oxygen and catalysts could be optimized to achieve higher propylene selectivity.¹³⁻¹⁹ Lastly, propane can be converted into propylene without catalysts via pyrolysis, which follows a free radical mechanism.²⁰⁻²² This route is highly endothermic and is thermodynamic limited. The reaction equilibrium can be shifted and the reaction rate can be

accelerated by adding H₂,²³⁻²⁴ phenyl radicals,²⁵ acetylene,²⁶ and ethylene.²⁷

Recently, oxidative dehydrogenation of propane without the addition of solid catalysts has been investigated.²⁸ The addition of NO in the feed was found to enhance propane conversion. It was hypothesized that there exists a redox cycle consisting of NO oxidation to NO₂, NO₂ hydrogenation to HONO, and HONO dissociation into NO and OH radicals. This cycle facilitates H-abstraction from propane and in turn increases propane conversion to propylene and other products. The hypothesized redox cycle is qualitatively supported by the experimental results, which showed that propane conversion increased with the amount of NO, O₂, and H₂O in the feed. However, no quantitative validation and detailed analysis of the hypothesized reaction pathways using the experimental findings were conducted.

In this work, a detailed kinetic model was constructed to elucidate the reaction pathways of gas-phase, homogeneous, NO_X-mediated oxidative dehydrogenation of propane free of solid catalysts. The species molar fractions as a function of downstream distance in plug flow reactors were simulated. The molar fractions of the key species at the exit of the reactor were compared to the experimental data for model validation. Detailed reaction pathways were also sketched to explain the important trends observed in the experiments.

Model Development

The detailed kinetic model was constructed by incorporating several published reaction mechanisms in the literature related to hydrocarbon combustion and NO_X formation. Specifically,

the Lawrence Livermore *n*-heptane combustion mechanism, ²⁹ consisting of 654 species and 2,827 elementary reactions, was used to describe propane oxidation. Since propane activation is expected to be critical in this reaction system, updated kinetic parameters for propane activation by HO₂ reported by Burluka et al.³⁰ were used instead (Reactions 1-2 in Table 1). Additional 108 reactions from the GRI-Mech 3.0 mechanism³¹ were also included to account for NO_X formation during hydrocarbon oxidation. Note that there exist newer NO_X formation mechanisms in the literature, as reviewed by Glarborg et al.³² These mechanisms, however, mainly focus on improving the formation chemistry of NO from gas-phase N₂ or nitrogen-containing fuels. The rate parameters of the interconversion reactions between NO and NO₂, which are believed to play a key role in our system, have not been significantly updated. Goldsmith et al. 33-35 studied reaction kinetics of light alkane (e.g., CH₄, C₂H₆, C₃H₈) oxidation in the presence of NO₂. They suggested that NO₂ can abstract a hydrogen atom from H₂ and these light alkanes to produce one of the three HONO isomers (trans-HONO, cis-HONO, and HNO₂), which rapidly dissociates into NO and OH radicals. To account for these pathways, 18 reactions describing H-abstraction by NO₂ to produce HONO isomers³³ and 13 reactions³⁶ describing the isomerization and dissociation of HONO isomers into NO and OH radicals were added (Table 1). In summary, our final reaction mechanism consists of 674 species and 2,966 elementary reactions. Note that in our mechanism, no ad hoc reactions were included, and there was no attempt to fit the kinetic parameters to any experimental data.

Table 1. Kinetic parameters of propane activation by HO₂ (Reactions 1 and 2),³⁰ H-abstraction by NO₂ to produce HONO isomers (Reactions 3–20),³³ and HONO isomerization and dissociation (Reactions 21–33).³⁶

	Reaction	A (in mol-cm-s-K units)	n	Ea (cal/mol)
1	$C_3H_8 + HO_2 = norm - C_3H_7 + H_2O_2$	4.76×10^4	2.55	16490
2	$C_3H_8 + HO_2 = iso-C_3H_7 + H_2O_2$	9.64×10^{3}	2.60	13910
3	$H_2 + NO_2 = H + cis-HONO$	1.21×10^{2}	3.29	28100
4	$H_2 + NO_2 = H + trans-HONO$	4.37×10^{2}	3.29	37100
5	$H_2 + NO_2 = H + HNO_2$	2.41×10^{4}	2.53	32700
6	$CH_4 + NO_2 = CH_3 + cis-HONO$	1.60×10^{0}	3.95	27800
7	$CH_4 + NO_2 = CH_3 + trans-HONO$	1.51×10^{1}	3.75	34700
8	$CH_4 + NO_2 = CH_3 + HNO_2$	6.87×10^{2}	3.16	32000
9	$C_2H_6 + NO_2 = C_2H_5 + cis-HONO$	3.32×10^{0}	3.84	23900
10	$C_2H_6 + NO_2 = C_2H_5 + trans-HONO$	8.49×10^{1}	3.45	32000
11	$C_2H_6 + NO_2 = C_2H_5 + HNO_2$	3.20×10^{2}	3.19	26500
12	$C_3H_8 + NO_2 = norm-C_3H_7 + cis-HONO$	2.47×10^{0}	3.83	24100
13	$C_3H_8 + NO_2 = norm-C_3H_7 + trans-HONO$	4.90×10^{1}	3.50	32600
14	$C_3H_8 + NO_2 = norm-C_3H_7 + HNO_2$	8.43×10^{1}	3.28	26500
15	$C_3H_8 + NO_2 = iso-C_3H_7 + cis-HONO$	1.65×10^{0}	3.69	21100
16	$C_3H_8 + NO_2 = iso-C_3H_7 + trans-HONO$	1.80×10^{1}	3.38	29800
17	$C_3H_8 + NO_2 = iso-C_3H_7 + HNO_2$	4.83×10^{1}	3.18	22700
18	$C_3H_6 + NO_2 = C_3H_5 - A + cis-HONO$	4.47×10 ⁻⁴	4.79	18100
19	$C_3H_6 + NO_2 = C_3H_5 - A + trans-HONO$	2.63×10 ⁻⁶	5.32	25200
20	$C_3H_6 + NO_2 = C_3H_5 - A + HNO_2$	2.54×10^{-2}	4.21	18700
21	$HNO_2 = cis-HONO$	1.56×10^{30}	-6.47	44360
22	$HNO_2 = trans-HONO$	1.56×10^{30}	-6.47	44360
23	OH + NO = cis-HONO	3.09×10^{23}	-4.17	1621
24	OH + NO = trans-HONO	3.09×10^{23}	-4.17	1621
25	$OH + NO = HNO_2$	1.43×10^{18}	-3.03	3899
26	$H + cis-HONO = NO + H_2O$	4.30×10^9	0.98	4070
27	$H + trans-HONO = NO + H_2O$	4.30×10^9	0.98	4070
28	$H + HNO_2 = NO + H_2O$	3.38×10^{9}	1.07	5565
29	$H + HNO_2 = HNO + OH$	3.65×10^{7}	1.78	5570
30	HNO + OH = H + cis-HONO	1.48×10^{3}	2.72	4554
31	HNO + OH = H + trans-HONO	1.48×10^{3}	2.72	4554
32	$HNO + NO_2 = NO + cis-HONO$	7.85×10^{2}	3.06	3882
33	$HNO + NO_2 = NO + trans-HONO$	7.85×10^{2}	3.06	3882

To enable comparison to the experimental data by Annamalai et al.,²⁸ plug flow reactor module in ANSYS Chemkin-Pro 19.2³⁷ was used. The simulated feed contains 3 kPa of propane, 10 kPa of oxygen, 0–0.03 kPa of NO, and 0–10 kPa of steam (i.e., H₂O vapor), with helium (He) as the balance gas to reach a total pressure of 1 atm. The modeled temperature was 773 K (500°C), with a total inlet gas flow rate of 15–110 ml/min. The simulated reactors have a diameter of 0.25 in, with two different lengths, 6.22 and 13.68 in, corresponding to heating zones of 5 and 11 cm³ in actual reactors of 6 and 12 cm³, respectively. Note that the actual reactors used in the experiments were U-shaped tubes. We assume that plug flows were developed in these reactors and heating zones were kept isothermally. Consequently, simple tubular reactors were used as an approximation in our simulations. In addition, gas temperature was modeled isothermally and uniformly at 773 K, although the flow rates of the inlet gas (in ml/min) were calculated based on standard conditions (i.e., 25°C and 1 atm).

Results and Discussion

Propane conversion and product selectivity. Figure 1 compares propane conversion predicted from the model to the experimental data for both 6 and 12 cm³ reactors. Both the model and the experiments suggest that propane conversion increases with NO pressure in the feed. The model and the experiments are in very good quantitative agreement.

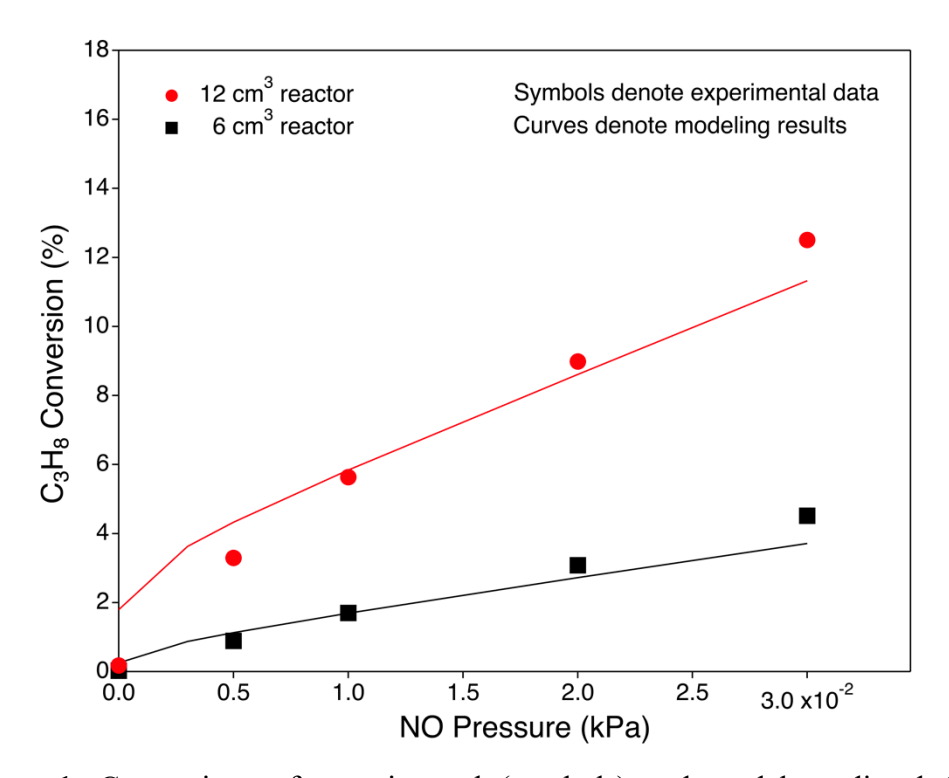


Figure 1. Comparison of experimental (symbols) and model predicted (curves) propane conversion as a function of NO pressure in the feed (reaction temperature: 773 K, He flow rate: 30 ml/min, C₃H₈: 3 kPa, O₂: 10 kPa, NO: 0–0.03 kPa, H₂O: 0 kPa)

Figure 2 compares model predicted selectivity of key products to the experimental values. Both the model and the experiments suggest that the selectivity of propylene, the target product, decreases with increasing propane conversion, with model predictions approximately 10% higher than the experimental values. Ethylene had the second highest selectivity in the experiments, which increases with propane conversion. However, the model predicted ethylene selectivity is lower

than the experimental values by approximately 10%. The magnitude of underprediction of ethylene selectivity is almost the same as the extent of overprediction of propylene selectivity, such that the combined selectivity of propylene and ethylene is nearly the same between the model and the experiments. This suggests that the model overpredicts the ratio of isopropyl (i-C₃H₇) to normal propyl (n-C₃H₇) radicals, where the former leads to the formation of propylene and the later leads to the formation of ethylene.²⁵

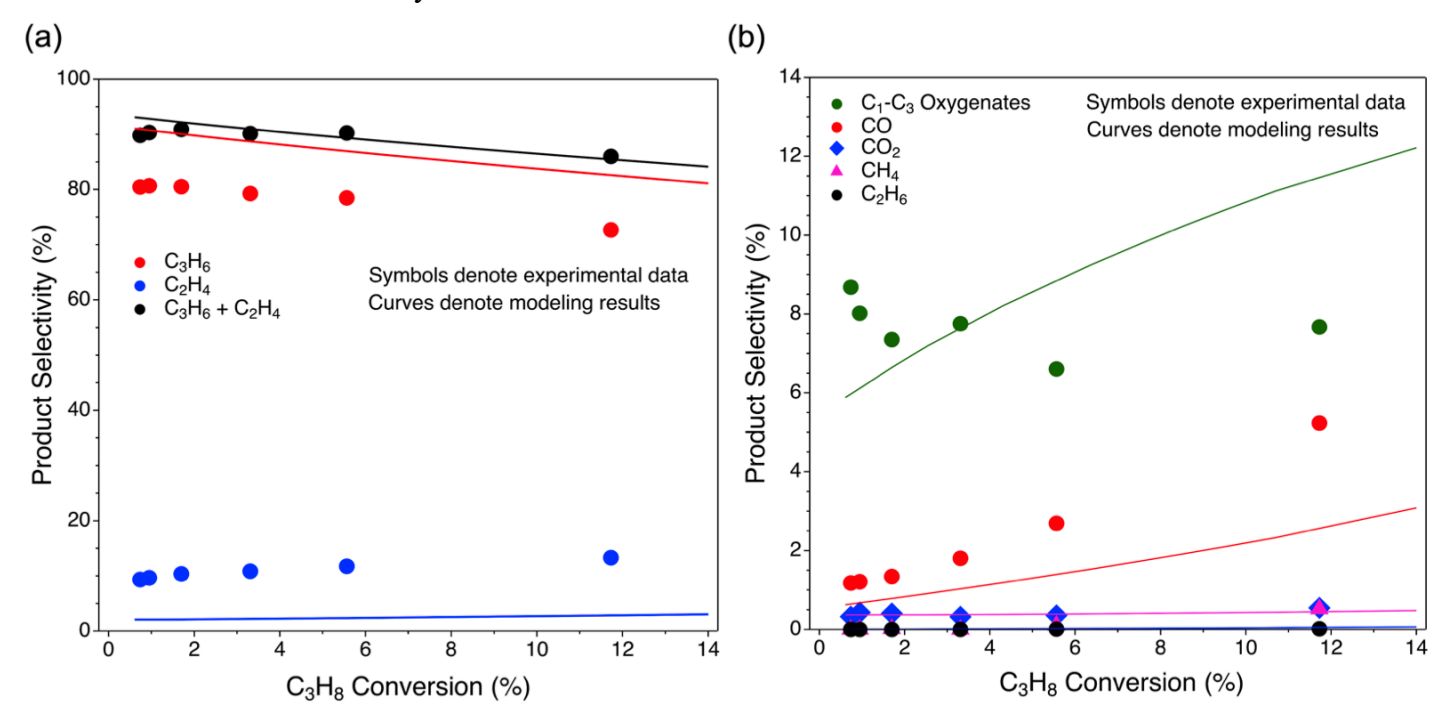


Figure 2. Comparison of the experimental (symbols) and model predicted (curves) selectivity of (a) propylene and ethylene and (b) other carbon-containing products as a function of propane conversion (reaction temperature: 773 K, He flow rate: 15–110 ml/min, C₃H₈: 3 kPa, O₂: 10 kPa, NO: 0.005 kPa, H₂O: 0 kPa, reactor size: 12 cm³).

The role of OH radicals. Figure 3a depicts model predicted propane conversion and product selectivity at the exit of the 12 cm³ reactor using five different feed compositions. The predicted molar fractions of OH radicals as a function of residence time for the five cases are shown in Figure

3b. In the case of propane pyrolysis (i.e., no O₂ present), regardless the presence of NO in the feed (Cases 1 and 2), propane conversion is nearly zero. This indicates that NO has no direct effect on propane pyrolysis, consistent with the fact that NO is a weak oxidant and is unlikely to abstract hydrogen directly from propane. In the presence of a strong oxidant in O₂ in the feed (at 10 kPa), propane conversion increases to 1.8% (Case 3), with a propylene selectivity of approximately 90%. This is accompanied by the formation of OH radicals in the system (Figure 3b), suggesting that Habstraction from propane by the OH radicals is the likely pathway leading to increased propylene production.²⁸ In the presence of both NO (at 0.03 kPa) and O₂ (at 10 kPa) in the feed (Case 4), propane conversion is significantly enhanced to approximately 11%, with the selectivity of propylene slightly decreased to 83%. There is also a higher OH molar fraction in this case, particularly a sharp peak of OH production at the very beginning of the reaction. The addition of 5 kPa of H₂O in the feed (Case 5) further increases propane conversion to approximately 18%, with the selectivity of propylene decreased to approximately 79%. The model also shows that the amount of OH radicals increase significantly in this case, particularly during longer reaction times. In summary, the increased propane conversion correlates well with the enhanced production of OH radicals over the course of the process, which is caused by the joint presence of NO and O₂ in the feed and promoted by the addition of H₂O.

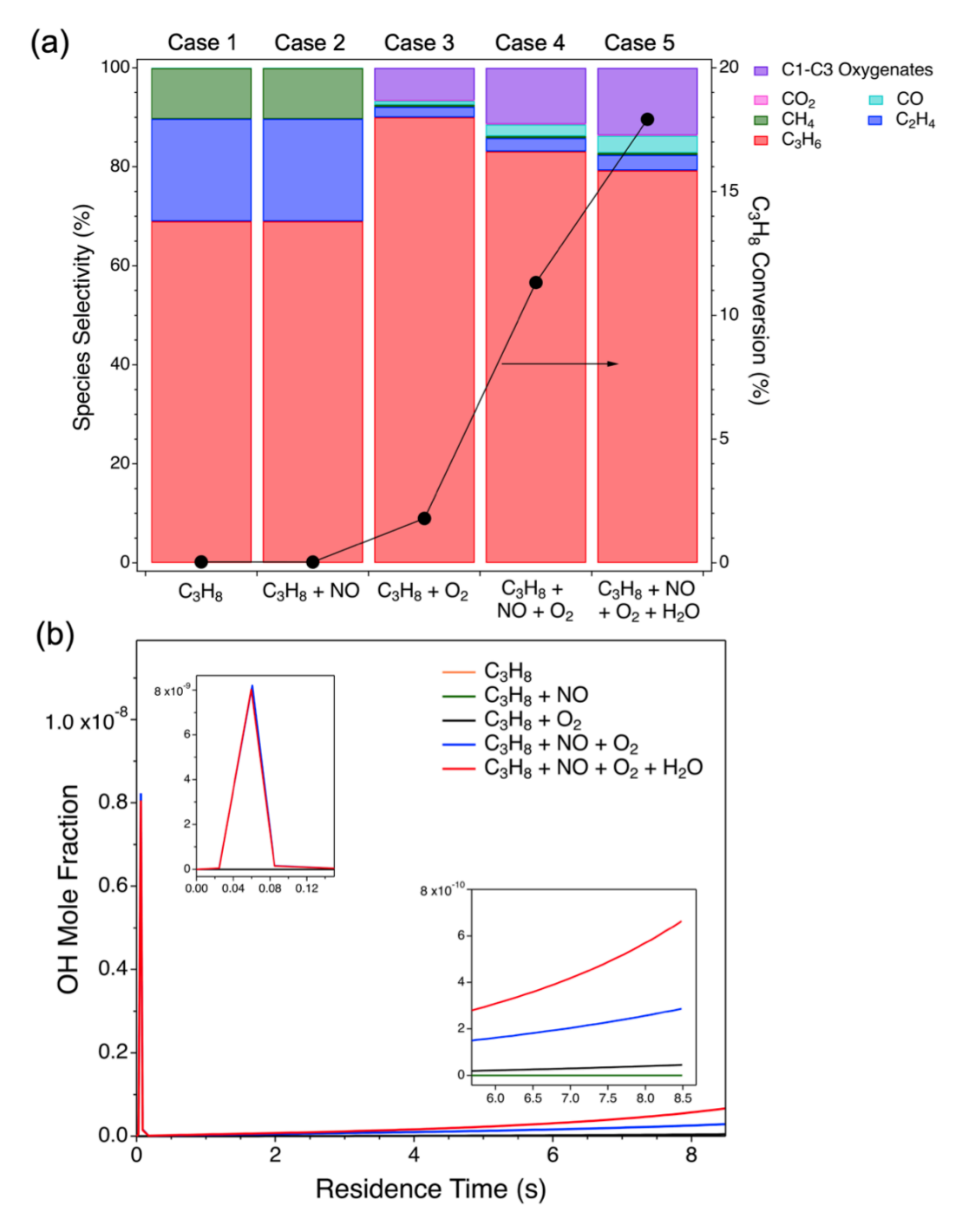


Figure 3. (a) Propane conversion and product selectivity and (b) molar fractions of OH radicals as a function of residence time predicted from the model using five different feed compositions: (1) propane pyrolysis (i.e., no O₂), (2) propane pyrolysis in the presence of NO at 0.03 kPa in the feed, (3) propane oxidation with a O₂ feed pressure at 10 kPa, (4) propane oxidation in the presence of NO at 0.03 kPa in the feed, (5) propane oxidation in the presence of both NO (0.03 kPa) and H₂O (5 kPa) in the feed (reaction temperature: 773 K, He flow rate: 30 ml/min, C₃H₈: 3 kPa, reactor size: 12 cm³).

Figure 4a depicts the model predicted molar fractions of propane and the major reaction products as a function of residence time. In this simulation, the initial feed was set as 3 kPa of propane, 10 kPa of O₂, 0.03 kPa of NO, no H₂O, and balanced He at 1 atm. Residence time of up to 50 s was tracked. As shown in Figure 4a, the molar fraction of propane decreases continuously and approaches zero at about 24 s. The molar fraction of the target product, propylene, reaches a maximum at approximately 16.5 s. This suggests that there is an optimal residence time to obtain the highest propylene yield. The entire reaction system reaches steady state at approximately 27 s, with major products being H₂O, CO, and CO₂, indicating incomplete combustion. Our model suggests that H-abstraction by OH radicals from propane to produce iso- and normal- propyl (C₃H₇) radicals are the primary pathways to consume propane (blue and red curves in Figure 4b). The rates of these reactions first peak immediately entering the reactor due to highest concentration of propane and the drastic increase of OH radicals (Figure 4c). This peak of OH radicals at the entrance is caused by the immediate NO oxidation into NO_2 ($HO_2 + NO = NO_2 + OH$), depicted by the dash blue curve in Figure 4d. There also exists a second peak of OH radicals that gradually increases until approximately 24 s (Figure 4c), resulting in continuing depletion of propane to produce propyl radicals (Figure 4b). As illustrated by Figure 4d, this second OH peak is firstly caused by H_2O_2 decomposition ($H_2O_2 = 2OH$) and ally radical (C_3H_5 -A) oxidation by HO_2 (C_3H_5 - $A + HO_2 = C_3H_5O + OH$) between 2 and 24 s, followed by both NO oxidation into NO₂ (HO₂ + $NO = NO_2 + OH$) and NO_2 reduction back to $NO (NO_2 + H = NO + OH)$ between 12 and 28 s. The quenching of the OH radicals after 24 s is primarily driven by oxidation pathways to produce CO₂ and H₂O (Figure 4e).

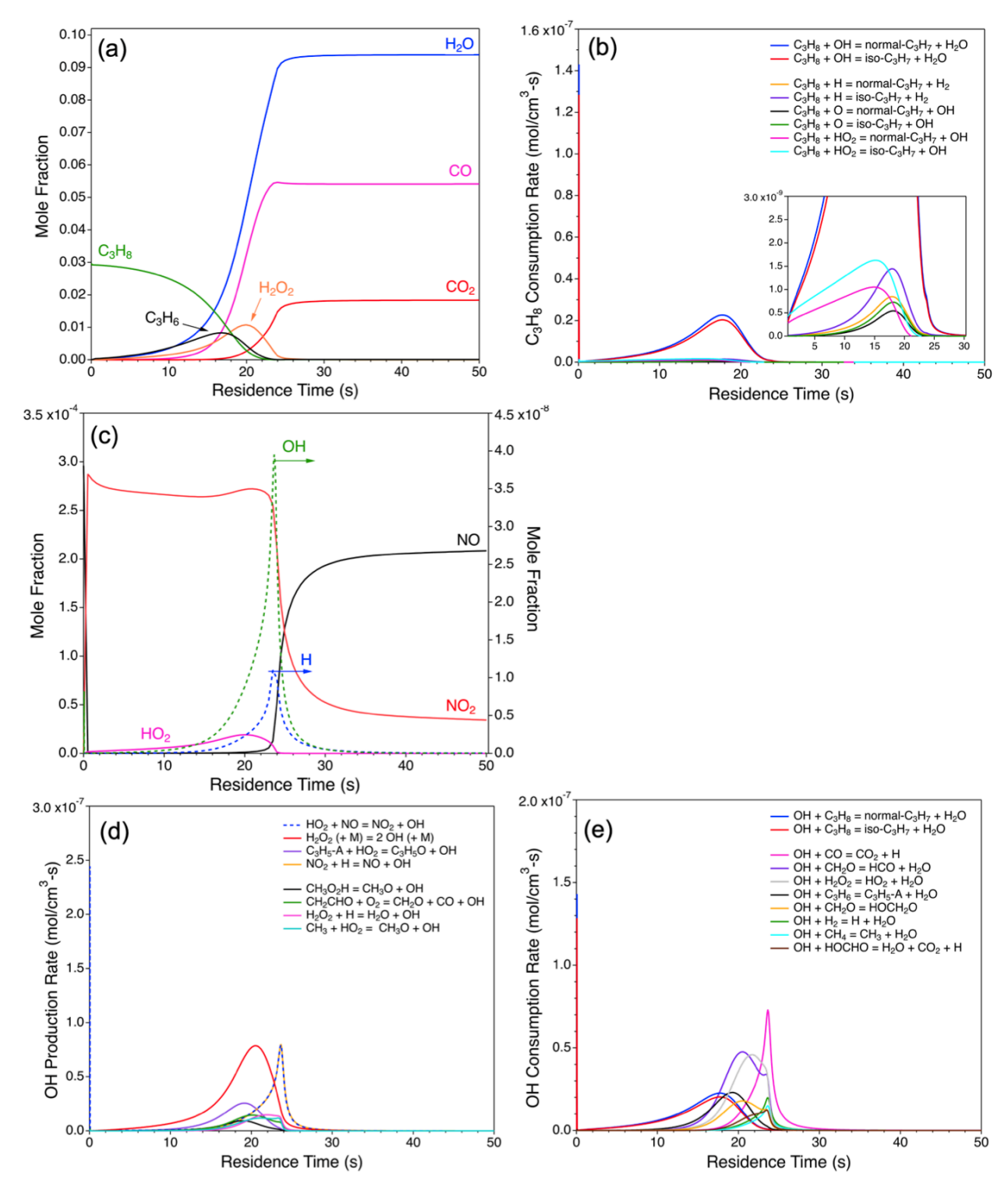


Figure 4. Model predicted time evolutions of (a) molar fractions of propane and the major products, (b) rates of the major propane consumption reactions, (c) molar fractions of NO, NO₂, and OH, H, and HO₂ radicals, (d) rates of the major OH production reactions, and (e) rates of the major OH consumption reactions (reaction temperature: 773 K, C₃H₈: 3 kPa, O₂: 10 kPa, NO: 0.03 kPa, H₂O: 0 kPa).

Table 2. List of components in different mechanisms studied in this work.

		Model A	Model B	Full Model
1	N-heptane combustion mechanism (2,827 reactions)	$\sqrt{}$	$\sqrt{}$	
2	NO _x reactions from GRI (108 reactions)	$\sqrt{}$	$\sqrt{}$	\checkmark
3	Reactions of H-abstraction by NO ₂ to produce HONO		2	2/
	(Reactions 3-20 in Table 1)		V	V
4	HONO dissociation reactions			ما
	(Reactions 21-33 in Table 1)			V

The NO-NO₂ cycle. Our modeling results in Figure 4 revealed that the main role of NO_X in oxidative dehydrogenation of propane is to promote the formation of OH radicals for increased propyl radical formation. To further elucidate the detailed effects of different NO_X species (i.e., NO, NO₂, and HONO isomers), two reaction mechanisms with several key pathways removed from the full mechanism, as listed in Table 2, were used for simulations. The first reaction mechanism (Model A) removes the formation and dissociation pathways of HONO and its isomers, while the second reaction mechanism (Model B) includes the HONO formation pathways without allowing HONO dissociation into NO and OH. Time evolutions of molar fractions of NO, NO₂, and critical radicals, including OH radicals, and rates of the major OH production and consumption reactions predicted from Models A and B are shown in Figure 5, which can be compared to the full model results in Figure 4.

Several findings were observed from this modeling exercise. First, the NO and OH molar fractions predicted from Model A (Figure 5a) are similar to those obtained from the full mechanism (Figure 4c). Note that Model A does not include H-abstraction reactions by NO₂, therefore no HONO or its isomers are formed. The addition of H-abstraction by NO₂ (Model B) lowers the

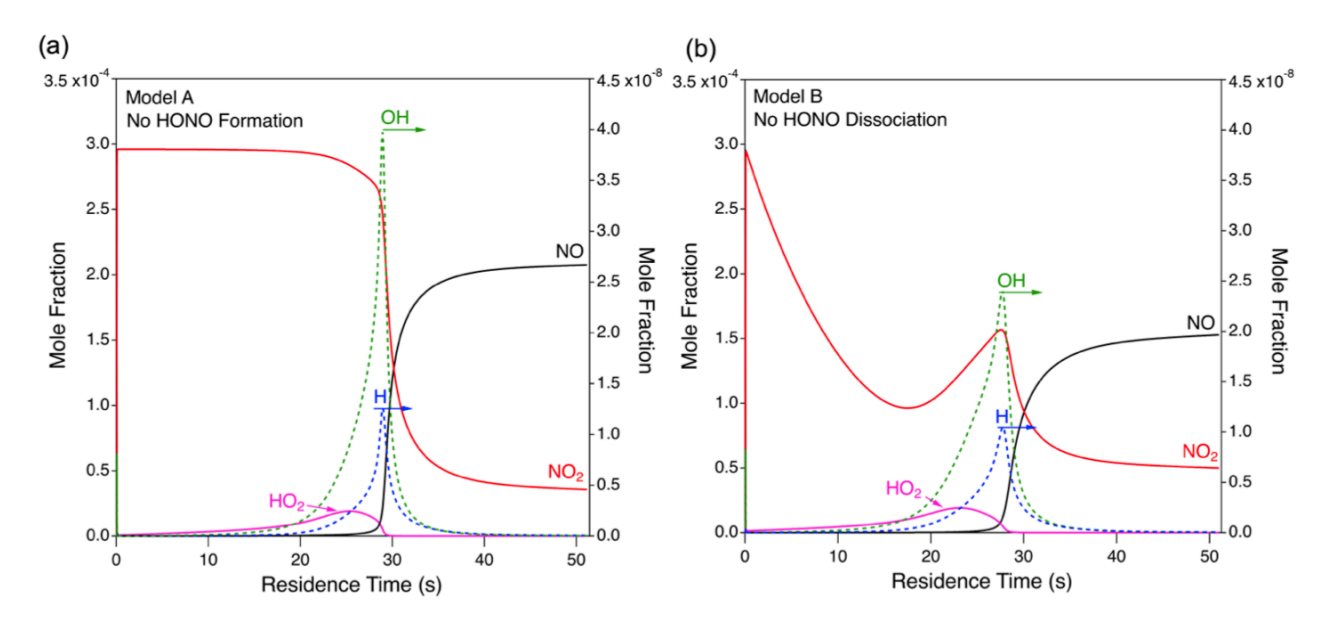


Figure 5. Time evolutions of molar fractions of NO, NO₂, and OH, H, and HO₂ radicals predicted from (a) Model A and (b) Model B.

molar fractions of NO₂ and OH (Figure 5b), where part of the NO₂ is consumed by H-abstraction reactions to produce HONO and its isomers. Since there is no HONO dissociation pathways in Model B, the second OH formation peak at approximately 27.5 s (Figure 5b) is lower compared to the full model (Figure 4c). The presence of the HONO dissociation pathways in the full model allows HONO and its isomers to dissociate into OH and NO. NO is then oxidized into NO₂ via reacting with HO₂. Both pathways generate more OH radicals. The additional production of OH radicals via the dissociation of HONO and isomers also explains why the second OH peak appears earlier in the full model (Figure 4c) compared to Model A (Figure 5a), which further results in increased propane conversion. In summary, the presence of NO_X in the reaction system facilitates propane conversion via two mechanisms (Figure 6): (1) continued generation of OH radicals via the NO–NO₂ redox cycle; (2) direct H-abstraction of propane by NO₂, which forms HONO and isomers that further dissociate into OH and NO.

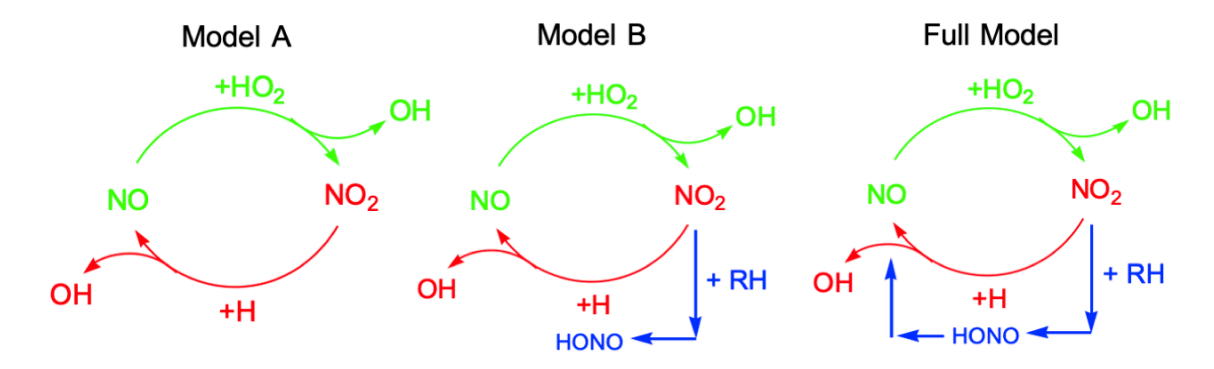


Figure 6. Schematic representation of NO–NO₂ cycle when Models A, B and the full model were exercised. The full model suggests that NO oxidation (green), NO₂ reduction (red), and HONO dissociation (blue) all contribute to the production of OH radicals.

To further confirm the effect of NO_X, simulations without the addition of NO in the feed was performed using the full model. Figure 7 shows the evolutions of molar fractions of the major species and the rates of major OH production reactions as a function of residence time. In the case of no NO in the feed, OH production (Figure 7a) appears to be later and slower than the case with NO (Figure 4c). In addition, there is no sharp peak associated with OH production due to NO oxidation into NO₂ at the entrance of the reactor (Figure 7b). These findings further confirm that

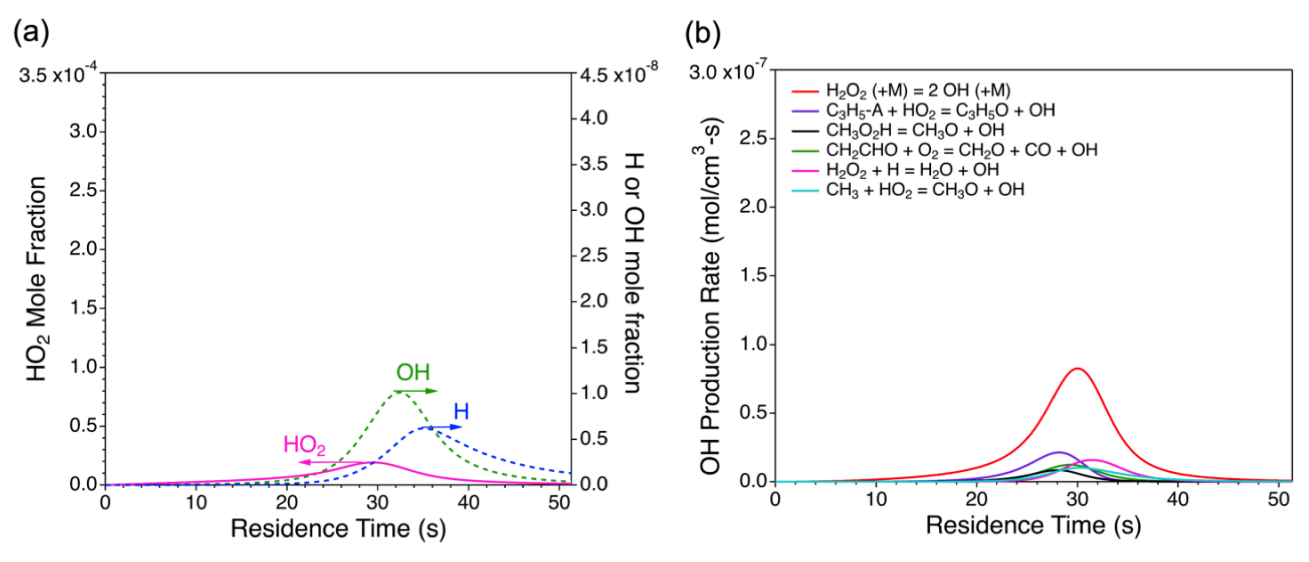


Figure 7. Time evolutions of (a) molar fractions of OH, H, and HO₂ radicals and (b) OH production rates as a function of residence time predicted from the full mechanism without NO in the feed (reaction temperature: 773 K, C₃H₈: 3 kPa, O₂: 10 kPa, NO: 0 kPa, H₂O: 0 kPa).

the addition of NO in the feed promotes the formation of OH radicals, which is the main reason contributing to enhanced propane conversion.

The effect of H₂O. As discussed earlier in Figure 3, the addition of H₂O significantly improves propane conversion and the amount of OH radicals in the system. The effect of H₂O was further studied with and without the addition of NO in our simulations, as shown in Figure 8. It was found that increased H₂O pressure in the feed increases propane conversion regardless of the presence of NO. The addition of H₂O also accelerates the chemistry, where the peak propylene molar fraction takes place at about 13 s (Figure 9), approximately 3.5 s earlier compared to that without H₂O in the feed (Figure 4a). The system also reaches equilibrium sooner at 22 s (Figure 9), as opposed to 27 s without H₂O in the feed (Figure 4a). Our simulation results suggest that the addition of H₂O

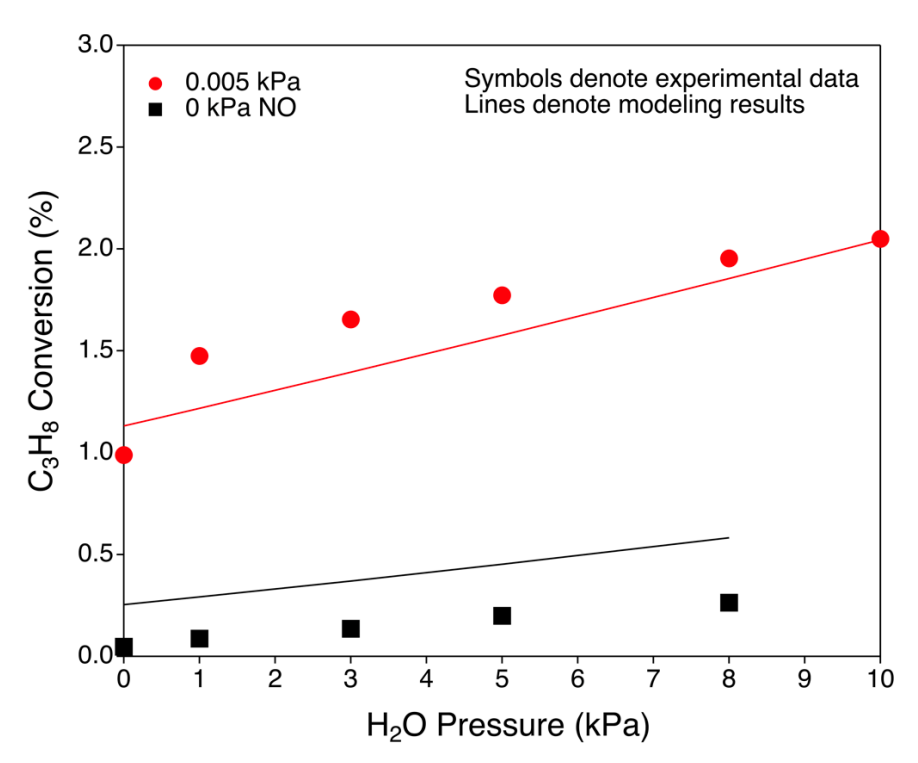


Figure 8. Comparison of experimental (symbols) and model predicted (lines) propane conversion as a function of H₂O pressure in the feed (reaction temperature: 773 K, He flow rate: 30 ml/min, C₃H₈: 3 kPa, O₂: 10 kPa, H₂O: 0–10 kPa, reactor size: 6 cm³).

shifts the equilibrium of OH quenching reactions where H₂O is the main product, accelerating the reaction pathways of propylene production.

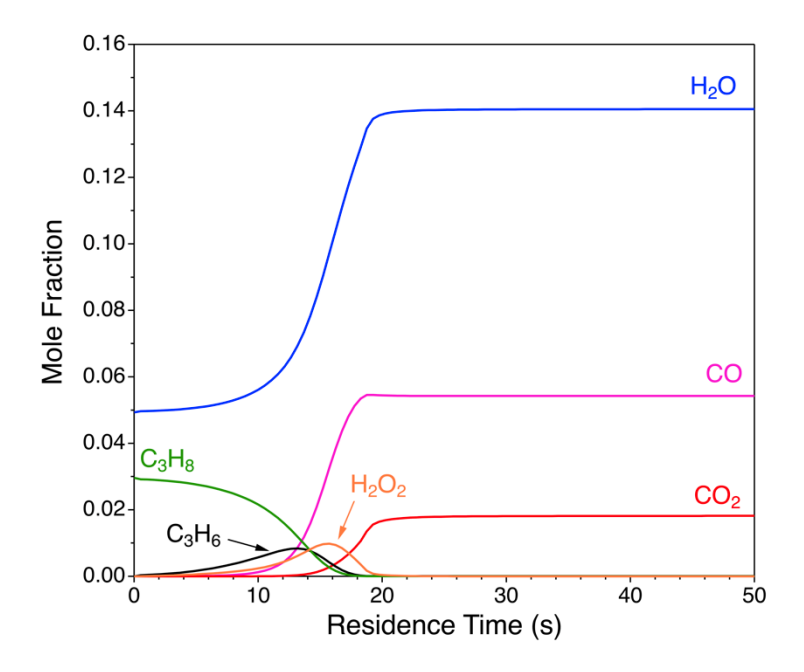


Figure 9. Model predicted molar fraction of major species as a function of residence time in the presence of H₂O in the feed (reaction temperature: 773 K, C₃H₈: 3 kPa, O₂: 10 kPa, NO: 0.03 kPa, H₂O: 5 kPa).

A reaction network of NO_X-mediated oxidative dehydrogenation of propane is sketched in Figure 10. The reaction is initialized by propane pyrolysis, in which C–C bonds and C–H bonds in propane are cleaved, forming methyl (CH₃), ethyl (C₂H₅), and iso/norm–propyl (C₃H₇) radicals. All the radicals can abstract a hydrogen atom from propane, leading to increased formation of propyl (C₃H₇) radicals that produce propylene and ethylene. The details of these pathways are discussed in our previous work.²⁵ In the presence of oxygen, the iso/norm–C₃H₇ radicals can react with O₂ to form iso/norm–C₃H₇O₂ radicals, which subsequently release propylene and HO₂. This is the major pathway for propylene production in the presence of O₂. Finally, the HO₂ radicals can

be converted into H₂O₂ by H-abstraction or serve as an oxidant in the NO–NO₂ cycle, both of which ultimately increase the amount of OH radicals, contributing to increased propane conversion.

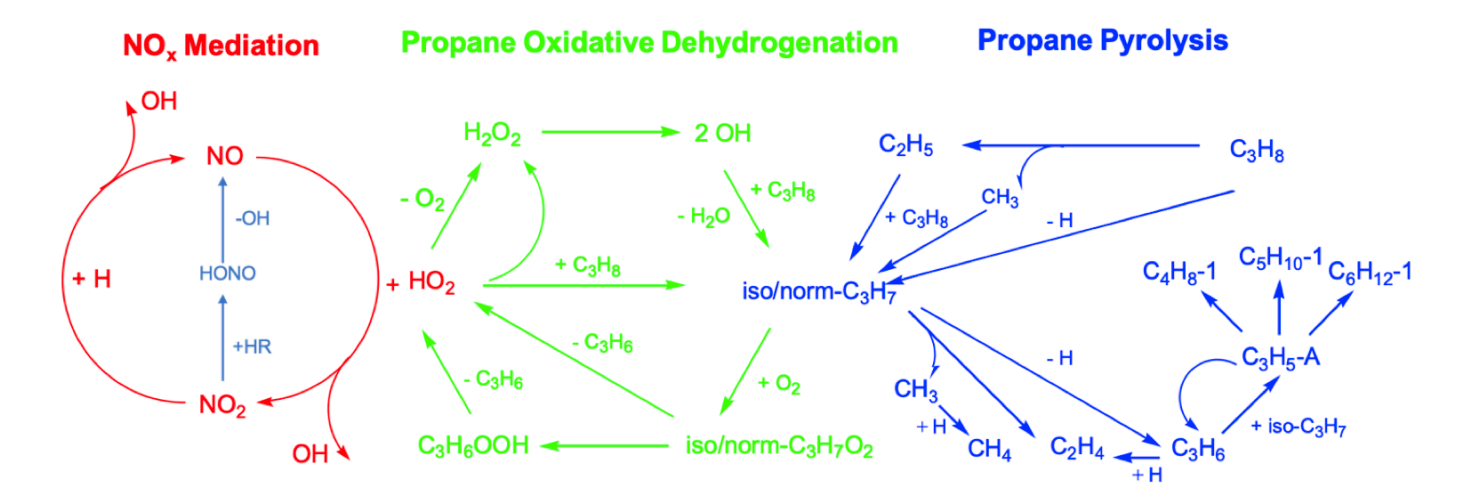


Figure 10. Reaction network of NO_X-mediated oxidative dehydrogenation of propane.

Conclusions

Oxidative dehydrogenation of propane mediated by NO_X has been studied by detailed kinetic modeling. The model shows that propane conversion increases with the amount of NO in the feed, and the selectivity to propylene and ethylene decreases with propane conversion. Both trends are agreeable with the experimental findings. The model also suggests that there is an optimal reaction time for achieving the highest propylene selectivity. The reaction reaches equilibrium with CO, CO₂, and H₂O as the final products. Detailed analysis revealed that OH radicals are the major species to activate propane. The addition of NO_X in the system provides additional amount of OH radicals through a NO–NO₂ cycle, which includes (1) oxidation of NO by HO₂ radicals to produce NO₂, (2) reduction of NO₂ by H radicals back to NO, and (3) formation of HONO and its isomers

by hydrogen abstraction of NO₂, followed by dissociation of HONO isomers into NO and OH. All

three pathways increase the amount of OH radicals and facilitate propane conversion. The addition

of H₂O accelerates the reactions by shifting the equilibrium of OH quenching. A reaction network,

consisting of detailed pathways of propane pyrolysis, propane oxidative dehydrogenation, and

NO_X mediation, was sketched to elucidate the mechanisms of propylene formation through NO_X-

mediated oxidative dehydrogenation of propane.

Acknowledgements

The authors are grateful for the funding support from the National Science Foundation (P.Y. and

H.W.: CBET-1842101; P.D. and Y.L: CBET-2034911)

19

References

- (1) Scott, J., ACC: White House Report Confirms Importance of Shale Gas to U.S. Manufacturing, Economic Revival. *American Chemistry Council* **2012**.
- (2) U.S. Energy Information Administration, Annual Energy Outlook 2018 with Projection to 2050. **2018**.
- (3) Sims, B., From Molecules to Products: Petrochemicals' Global Rise. *FUEL* **2015**.
- (4) International Energy Agency, The future of Petrochemicals Toward more sustainable plastics and fertilizers. **2018**.
- (5) Alper, J.; Rapporteur, The Changing Landscape of Hydrocarbon Feedstocks for Chemical Production: Implications for Catalysis: Proceedings of a Workshop. *The national Academies Press* **2016**.
- (6) Boswell, C., On-purpose technologies ready to fill propylene gap. *Independent Commodity Inteligence Services* **2012**.
- (7) Bariås, O. A.; Holmen, A.; Blekkan, E. A., Propane dehydrogenation over supported Pt and Pt–Sn catalysts: catalyst preparation, characterization, and activity measurements. *Journal of Catalysis* **1996**, *158* (1), 1-12.
- (8) Zhang, Y.; Zhou, Y.; Qiu, A.; Wang, Y.; Xu, Y.; Wu, P., Propane dehydrogenation on PtSn/ZSM-5 catalyst: Effect of tin as a promoter. *Catalysis Communications* **2006**, *7* (11), 860-866.
- (9) Zhang, Y.; Zhou, Y.; Shi, J.; Zhou, S.; Sheng, X.; Zhang, Z.; Xiang, S., Comparative study of bimetallic Pt-Sn catalysts supported on different supports for propane dehydrogenation.

- Journal of Molecular Catalysis A: Chemical 2014, 381, 138-147.
- (10) Yu, C.; Ge, Q.; Xu, H.; Li, W., Effects of Ce addition on the Pt-Sn/γ-Al₂O₃ catalyst for propane dehydrogenation to propylene. *Applied Catalysis A: General* **2006**, *315*, 58-67.
- (11) Zheng, B.; Hua, W.; Yue, Y.; Gao, Z., Dehydrogenation of propane to propene over different polymorphs of gallium oxide. *Journal of Catalysis* **2005**, *232* (1), 143-151.
- (12) Zhu, H.; Anjum, D. H.; Wang, Q.; Abou-Hamad, E.; Emsley, L.; Dong, H.; Laveille, P.; Li, L.; Samal, A. K.; Basset, J.-M., Sn surface-enriched Pt-Sn bimetallic nanoparticles as a selective and stable catalyst for propane dehydrogenation. *Journal of Catalysis* 2014, 320, 52-62.
- (13) Lemonidou, A.; Nalbandian, L.; Vasalos, I., Oxidative dehydrogenation of propane over vanadium oxide based catalysts: Effect of support and alkali promoter. *Catalysis Today* **2000,** *61* (1-4), 333-341.
- (14) Argyle, M. D.; Chen, K.; Bell, A. T.; Iglesia, E., Effect of catalyst structure on oxidative dehydrogenation of ethane and propane on alumina-supported vanadia. *Journal of Catalysis* **2002**, *208* (1), 139-149.
- (15) Grant, J.; Carrero, C. A.; Goeltl, F.; Venegas, J.; Mueller, P.; Burt, S. P.; Specht, S.; McDermott, W.; Chieregato, A.; Hermans, I., Selective oxidative dehydrogenation of propane to propene using boron nitride catalysts. *Science* **2016**, *354* (6319), 1570-1573.
- (16) Chen, K.; Bell, A. T.; Iglesia, E., Kinetics and mechanism of oxidative dehydrogenation of propane on vanadium, molybdenum, and tungsten oxides. *The Journal of Physical Chemistry B* **2000**, *104* (6), 1292-1299.

- (17) Corma, A.; Nieto, J. L.; Paredes, N., Influence of the preparation methods of V-Mg-O catalysts on their catalytic properties for the oxidative dehydrogenation of propane. *Journal of Catalysis* **1993**, *144* (2), 425-438.
- (18) Khodakov, A.; Yang, J.; Su, S.; Iglesia, E.; Bell, A. T., Structure and properties of vanadium oxide-zirconia catalysts for propane oxidative dehydrogenation. *Journal of Catalysis* **1998**, 177 (2), 343-351.
- (19) Atanga, M. A.; Rezaei, F.; Jawad, A.; Fitch, M.; Rownaghi, A. A., Oxidative dehydrogenation of propane to propylene with carbon dioxide. *Applied Catalysis B:*Environmental 2018, 220, 429-445.
- (20) Allara, D.; Edelson, D., A computational modeling study of the low-temperature pyrolysis of n-alkanes; mechanisms of propane, n-butane, and n-pentane pyrolyses. *International Journal of Chemical Kinetics* **1975**, *7* (4), 479-507.
- (21) Hidaka, Y.; Oki, T.; Kawano, H., Thermal decomposition of propane in shock waves.

 *International Journal of Chemical Kinetics 1989, 21 (8), 689-701.
- (22) Laidler, K.; Sagert, N.; Wojciechowski, B., Kinetics and mechanisms of the thermal decomposition of propane I. The Uninhibited of reaction. *Proceedings of the Royal Society of London. Series A. Mathematical Physical Sciences* **1962**, *270* (1341), 242-253.
- (23) Kamiński, A.; Sobkowski, J., Pyrolysis of propane in the presence of hydrogen. *Reaction Kinetics Catalysis Letters* **1981**, *16* (2-3), 105-109.
- (24) Ma, J.; Su, B.; Wen, G.; Ren, Q.; Yang, Y.; Yang, Q.; Xing, H., Kinetic modeling and experimental validation of the pyrolysis of propane in hydrogen plasma. *International*

- Journal of Hydrogen Energy **2016**, 41 (48), 22689-22697.
- (25) Yu, P.; Wong, H.-W., Propane pyrolysis facilitated by phenyl radicals: A combined experimental and kinetic modeling study. *Chemical Engineering Science* **2019**, *210*, 115243.
- (26) Kamiński, A., Pyrolysis of propane in the presence of acetylene. *Reaction Kinetics Catalysis Letters* **1992**, *48* (1), 309-313.
- (27) Pogosyan, N.; Pogosyan, M. D.; Arsentiev, S.; Tavadyan, L.; Strekova, L.; Arutyunov, V., Propylene Synthesis by Copyrolysis of Propane and Ethylene. *Petroleum Chemistry* **2020**, 60, 316-320.
- (28) Annamalai, L.; Liu, Y.; Deshlahra, P., Selective C–H Bond Activation via NOx-Mediated Generation of Strong H-Abstractors. *Acs Catalysis* **2019**, *9* (11), 10324-10338.
- (29) Curran, H. J.; Gaffuri, P.; Pitz, W. J.; Westbrook, C. K., A comprehensive modeling study of n-heptane oxidation. *Combustion flame* **1998**, *114* (1-2), 149-177.
- (30) Burluka, A. A.; Harker, M.; Osman, H.; Sheppard, C. G. W.; Konnov, A. A., Laminar burning velocities of three C₃H₆O isomers at atmospheric pressure. *Fuel* **2010**, *89* (10), 2864-2872.
- (31) Smith, G. P.; Golden, D. M.; Frenklach, M.; Moriarty, N. W.; Eiteneer, B.; Eiteneer, B.; Bowman, C. T.; Hanson, R. K.; Song, S.; Gardiner, J. W. C.; Lissianski, V. V.; Qin, Z., GRI-Mech 3.0. http://www.me.berkeley.edu/gri-mech/ 1999.
- (32) Glarborg, P.; Miller, J. A.; Ruscic, B.; Klippenstein, S. J., Modeling nitrogen chemistry in combustion. *Progress in Energy and Combustion Science* **2018**, *67*, 31-68.

- (33) Chai, J.; Goldsmith, C. F., Rate coefficients for fuel+NO₂: Predictive kinetics for HONO and HNO₂ formation. *Proceedings of the Combustion Institute* **2017**, *36* (1), 617-626.
- (34) Fuller, M. E.; Goldsmith, C. F., On the relative importance of HONO versus HNO₂ in low-temperature combustion. *Proceedings of the Combustion Institute* **2019**, *37* (1), 695-702.
- (35) Chen, X.; Fuller, M. E.; Goldsmith, C. F., Decomposition kinetics for HONO and HNO₂.

 *Reaction Chemistry Engineering 2019, 4 (2), 323-333.
- (36) Wang, Q.-D.; Sun, Y.; Curran, H. J., Comparative Chemical Kinetic Analysis and Skeletal Mechanism Generation for Syngas Combustion with NOx Chemistry. *Energy and Fuels* **2019**, *34* (1), 949-964.
- (37) ANSYS Chemkin-Pro Release 19.2, ANSYS, Inc.: Canonsburg, PA, **2018**, https://www.ansys.com/products/fluids/ansys-chemkin-pro.